

MULTISCALE MECHANICS GROUP (MSM)/TS/CTW
UNIVERSITY OF TWENTE, ENSCHEDE, NETHERLANDS
FEBRUARY 7, 2012

VICI Report (Project No. 10828)

To: VICI and Industrial Partners of project VICI No. 10828

From: Brian P. Lawney, Postdoc

Subject: Bridging the gap between particulate systems and continuum theory

Frequency filtering in disordered granular chains subject to harmonic driving

Brian P. Lawney Stefan Luding

February 7, 2012

Abstract

The study of disorder induced frequency filtering is presented for one-dimensional systems composed of random, pre-stressed masses interacting through both linear and nonlinear (Hertzian) repulsive forces. We drive an ensemble of such systems at a specified frequency and examine the frequency content of the propagated disturbance as a function of distance from the source. It is shown that the transmitted signal contains only low-frequency components and the attenuation is dependent on the magnitude of disorder, the input frequency, and the contact model. Normal, uniform, and binary distributions of mass are considered and observed to produce similar filtering behavior, suggesting that only knowledge of the distribution's moments is significant in characterizing the bulk signal transmission behavior of these systems.

1 Introduction

One-dimensional analogs of electronic, magnetic, and mechanical systems are often employed for their use as simple models which have the potential to reveal the physics of more general, higher dimensional systems [21]. As a subset of these problems, chains of non-cohesive particles have received significant attention in the literature. Linear arrangements of harmonic oscillators are common in the introduction to lattice vibrations in solid state physics [1, 11]. These treatments are typically limited to infinitely repeatable unit cells containing one or two particles/atoms for which dispersion equations relating the oscillation frequency and wavelength are analytically accessible. It is from these periodic, linear systems that more recent studies on inhomogeneous, disordered, and nonlinear chains originate.

The introduction of nonlinear (e.g., Hertzian) particle interactions resembles most experiments with granular chains of pre-stressed elastic spheres, and leads to novel behavior such as soliton-like nonlinear waves [3, 16, 23–25, 30, 36]. Sen *et al.* [35] provides a detailed account of prior studies concerning solitary waves in granular chains. Note that many studies focus on uncompressed chains where particles are barely in contact. Additionally, there is significant attention placed on the behavior of “designed” and ordered nonlinear chains, often motivated by energy modification and shock-protection applications. Studies have employed smoothly varying mass distributions [32], “decoration” [10, 12, 13], tapering [6, 26, 39, 41], and controlled variation of the particle material [4, 14]. Combinations of both tapering and decoration have also been employed [7, 12].

The inclusion of disorder through mass, size, or interaction (stiffness) variation (and combinations thereof) is a natural extension reflecting the disordered, inhomogeneous state of many realistic discrete systems. One-dimensional systems provide a simple framework to study the basic effects of disorder without consideration for the geometric complexity of higher dimensions, thus excluding the scattering of signals to other directions. Analysis of the spectrum and density of eigenstates was the subject of many early studies in disordered one-dimensional systems [5, 8, 27, 34]. In the context of quantum mechanical particles, Anderson [2] noted the localization of the wavefunctions in the presence of sufficiently strong random potentials. This “Anderson localization” has been confirmed in disordered mechanical systems of vibrating masses [20, 33].

As with tapered and decorated chain arrangements, recent studies of random granular arrays show an interest in the use of these systems to dissipate or enhance energy propagation. Nesterenko [30] examined the downstream speed and energy of particles in nonlinear random chains following an initial excitation applied to one end of the system. It was reasoned that complex nonlinear interactions between the chain members make the system behavior difficult to predict in general. Manciu *et al.* [25] reports a spatially exponential decrease of the incident kinetic energy for various amounts of mass disorder, with increasing disorder leading to a faster energy loss. Fraternali *et al.* [9] employed an evolutionary algorithm which generated random “protecting” chains whose effectiveness was evaluated by the force transmitted at the end of the system. It was noted that temporally short and high amplitude pulses were transformed to low amplitude, longer wavelength (temporally longer) signals at the downstream receiver. Ponson *et al.* [31] employs a nonlinear chain of two-particle unit cells which are randomly oriented, as in a spin system, and studies the effect of their disorder parameter on the spatial decay of the force transmitted by such systems. Harbola *et al.* [13] decorate monodisperse chains with randomly sized small masses and investigate the propagation time and decay of the pulse velocity as a function of system penetration.

Studies concerning the frequency-filtering effects of disorder have received less attention than energy or force attenuation. Jia *et al.* [15] reports experimental studies on ultrasound propagation through three-dimensional packings of glass beads. The time and frequency analysis of the transmitted signal reveals the appearance of an initial pulse close to the source that contains relatively low frequencies with respect to the input spectrum. The initial pulse is followed by an irregular signal, *i.e.* the “coda”, that contains the higher frequencies, consistent with the lower phase velocity of higher frequency components. The spectrum of this irregular signal seems to indicate more attenuation of the high frequency components. Judge *et al.* [17] numerically examine the spectra of disordered micromechanical oscillators, focusing on frequency filtering within the passband of ordered arrays. They note the significant change in the transmitted spectrum with increasing disorder and the propagation of frequencies associated with the natural frequency of the individual oscillators. The low-pass filtering seen does not seem to be observed, likely due to the short length of the arrays considered (5 oscillators). Mouraille and Luding [28, 29] numerically studied the high-frequency filtering present in three-dimensional packings perturbed from their perfect crystalline geometry by a small random variation in the particle sizes. Following a delta-like pulse of the boundary, only the low-frequency components of the excitation are observed to propagate a significant distance.

The polydispersity introduced is quite small with respect to the particle length scale (0.2% variation), but as this change is comparable to the contact length scale remarkable differences in the propagation characteristics of the medium are observed.

It is worth noting that nonlinear particle interactions permit frequency mixing behavior. Given excitations at frequencies ω_1 and ω_2 , a component at the difference-frequency $|\omega_2 - \omega_1|$ is generated, among others. For sufficiently close magnitudes, this is a low-frequency component. In realistic materials, the high-frequencies are attenuated and only the difference-frequency is seen to propagate a significant distance. Tournat *et al.* [40] observe the propagation of these low-frequency signals in nonlinear chains, terming it self de-modulation. However, such behavior is due to nonlinear interaction and is not a mass-disorder induced effect. Frequency mixing due to disorder was also noted by Mouraille [28].

In this paper we study the effect of disorder and non-linearity on the transmission of signals in one-dimensional systems. We consider initially static, pre-stressed configurations with given disorder magnitude that are subjected to a harmonic perturbation of the boundary. Prescribing a perturbation frequency, we average over many configurations of the chain to observe ensemble averaged behavior. In section 2 we derive the equations of motion that govern the idealized system. In particular, the linear and Hertzian force models are given in sections 2.1.2 and 2.1.3, respectively. Using these relations, we examine the effects of disorder on the high-frequency filtering behavior in section 3, and summarize and conclude in Section 4.

2 Modeling

In this section the equations of motion are derived employing a general nonlinear force-displacement relation. Two specific cases follow, corresponding to the harmonic (linear) and Hertzian models.

2.1 Compressed chain

In this study we consider one-dimensional arrays of $(N + 2)$ random mass particles which interact with only their immediate neighbors in a purely repulsive manner. In addition, we consider chains that are pre-compressed such that there is some initial strain associated with the equilibrium configuration. The absolute position, radius, and mass of a general particle j are given by $\tilde{x}^{(j)}$, $\tilde{r}^{(j)}$, and $\tilde{m}^{(j)}$, respectively. Anticipating an appropriate scaling of the problem, we employ the tilde symbols to denote dimensional quantities. The interaction force between neighboring particles i and j is modeled as,

$$\left| \tilde{F}_{(i,j)} \right| = \tilde{\kappa}_{(i,j)} \tilde{\delta}_{(i,j)}^{1+\beta}, \quad \tilde{\delta}_{(i,j)} \geq 0, \quad (1)$$

where $\tilde{\kappa}_{(i,j)}$ is a “stiffness” that changes with the value of β and depends, in general, on the properties of the contacting bodies. The particle overlap is given as $\tilde{\delta}_{(i,j)} = \tilde{r}^{(i)} + \tilde{r}^{(j)} - |\tilde{x}^{(j)} - \tilde{x}^{(i)}|$ such that it is strictly non-negative for contacts. The Hertz and linear models are given by $\beta = 1/2$ and $\beta = 0$, respectively [19, 22, 30]. Choosing a length scale $\tilde{\ell}$ (to be determined later) we

scale the particle overlap:

$$\left| \tilde{F}_{(i,j)} \right| = \tilde{\kappa}_{(i,j)} \tilde{\ell}^{1+\beta} \delta_{(i,j)}^{1+\beta}, \quad (2)$$

where $\delta_{(i,j)} \equiv \tilde{\delta}_{(i,j)}/\tilde{\ell}$. Compressing the chain by an applied force \tilde{P} , the dimensionless initial particle overlap at the contact between i and j is,

$$\Delta_{(i,j)} = \left(\frac{\tilde{P}}{\tilde{\kappa}_{(i,j)} \tilde{\ell}^{1+\beta}} \right)^{1/(1+\beta)}. \quad (3)$$

Associated with the length scale $\tilde{\ell}$, we have a characteristic mass \tilde{m}_o , which we take as the mean particle mass of the system. Dimensional analysis yields a time scale,

$$\tilde{t}_c = \frac{1}{\tilde{\ell}^{\beta/2}} \sqrt{\frac{\tilde{m}_o}{\tilde{\kappa}_o}}, \quad (4)$$

where $\tilde{\kappa}_o$ functions as the characteristic stiffness of the system. This will be defined with respect to the contact of two identical particles of the mean mass, \tilde{m}_o . In the nonlinear cases ($\beta \neq 0$) $\tilde{\ell}$ factors into this time scale. We may write an equation of motion for the general particle i ($i = 1, \dots, N$) as:

$$\tilde{m}^{(i)} \frac{d^2 \tilde{x}^{(i)}}{d\tilde{t}^2} = \tilde{\kappa}_{(i-1,i)} \tilde{\ell}^{1+\beta} \delta_{(i-1,i)}^{1+\beta} - \tilde{\kappa}_{(i+1,i)} \tilde{\ell}^{1+\beta} \delta_{(i+1,i)}^{1+\beta}. \quad (5)$$

We denote the displacement of particle i from its equilibrium position $\tilde{x}_o^{(i)}$ as $\tilde{u}^{(i)} = \tilde{\ell} u^{(i)} = \tilde{x}^{(i)} - \tilde{x}_o^{(i)}$. Thus, for a contact between i and j (with $j > i$) the scaled overlap is $\delta_{(i,j)} = \Delta_{(i,j)} - (u^{(j)} - u^{(i)})$. With dimensionless mass $b^{(i)} \equiv \tilde{m}^{(i)}/\tilde{m}_o$ and time $\tau \equiv \tilde{t}/\tilde{t}_c$ we write

$$b^{(i)} \frac{d^2 u^{(i)}}{d\tau^2} = \kappa_{(i-1,i)} \left[\Delta_{(i-1,i)} - u^{(i)} + u^{(i-1)} \right]^{1+\beta} - \kappa_{(i+1,i)} \left[\Delta_{(i+1,i)} + u^{(i)} - u^{(i+1)} \right]^{1+\beta}, \quad (6)$$

where the stiffness ratio $\kappa_{(i,j)} = \tilde{\kappa}_{(i,j)}/\tilde{\kappa}_o$ has been defined implicitly.

For the particles 1 and N we write equations of motion associated with the imposed boundary conditions. We harmonically displace particle 0 at angular frequency $\omega_o = \tilde{\omega}_o \tilde{t}_c$ and fix particle $(N+1)$:

$$u^{(0)}(\tau) = \epsilon \sin \omega_o \tau, \quad (7)$$

$$u^{(N+1)}(\tau) = 0, \quad (8)$$

where $\epsilon = \tilde{\epsilon}/\tilde{\ell}$ is the scaled oscillation amplitude. Thus, the coupled system of differential equations governing the modeled system is given by (6) with substitution of (7) and (8) for $i = 1$ and $i = N$, respectively.

There are various choices available for the length scale $\tilde{\ell}$. One could use the particle size or the driving amplitude. However, we choose the length scale to be related to the overlap of a characteristic contact in static equilibrium. As in defining the characteristic stiffness, we consider the contact of two identical particles of the mean mass. Under the applied compressive force, the initial

overlap between such particles provides us with $\tilde{\ell} = \tilde{\Delta}_o$ ($\Delta_o = 1$). In a typical simulation, the scaled driver amplitude $\epsilon \ll \Delta_o$ is chosen so as not to cause an opening of contacts. However, we explore driver amplitudes that approach the contact length scale under the restriction that particles remain in contact at all times. Note that ϵ incorporates the pre-compression of the system through (3):

$$\epsilon = \frac{\tilde{\epsilon}}{\tilde{\Delta}_o} = \tilde{\epsilon} \left(\frac{\tilde{\kappa}_o}{\tilde{P}} \right)^{2/3}. \quad (9)$$

Since $\tilde{\kappa}_o$ is set by the size of the particles (see Appendix B), small values of ϵ represent systems with small driving and/or a large pre-stress through \tilde{P} .

2.1.1 Linearized equations of motion:

Here we linearize the general force-displacement relation about the equilibrium configuration. The non-dimensional phrasing of (1) is given by

$$F_{(i,j)}(\delta_{(i,j)}) = \kappa_{(i,j)} \delta_{(i,j)}^{1+\beta}, \quad (10)$$

Expanding about the equilibrium position $\Delta_{(i,j)}$ we obtain,

$$F_{(i,j)}(\delta_{(i,j)}) = \kappa_{(i,j)} \Delta_{(i,j)}^{1+\beta} + \kappa_{(i,j)} (1 + \beta) \Delta_{(i,j)}^\beta (\delta_{(i,j)} - \Delta_{(i,j)}) + \frac{\kappa_{(i,j)} \beta (1 + \beta) \Delta_{(i,j)}^{\beta-1}}{2} (\delta_{(i,j)} - \Delta_{(i,j)})^2 + \dots \quad (11)$$

Assuming small displacements from equilibrium, we retain only the constant and linear terms. With $\delta_{(i,j)} = \Delta_{(i,j)} - (u^{(j)} - u^{(i)})$ for particle indices such that $j > i$ we obtain

$$F_{(i,j)}(\delta_{(i,j)}) = \kappa_{(i,j)} \Delta_{(i,j)}^{1+\beta} - \kappa_{(i,j)} (1 + \beta) \Delta_{(i,j)}^\beta (u^{(j)} - u^{(i)}), \quad (12)$$

which is the linearized force of particle i on particle j for $j > i$. The equation of motion for a general particle i is then,

$$b^{(i)} \frac{d^2 u^{(i)}}{d\tau^2} = \kappa_{(i-1,i)} \Delta_{(i-1,i)}^\beta \left[\Delta_{(i-1,i)} - (1 + \beta)(u^{(i)} - u^{(i-1)}) \right] - \kappa_{(i+1,i)} \Delta_{(i+1,i)}^\beta \left[\Delta_{(i+1,i)} - (1 + \beta)(u^{(i+1)} - u^{(i)}) \right]. \quad (13)$$

2.1.2 Linear coupling: $\beta = 0$

In the case of $\beta = 0$ we recover the harmonic chain with linear springs between the mass elements. Such a model is appropriate for realistic chains with sufficiently high confining force; Sinkovits *et al.* [38] show that the frequency spectrum of oscillations approaches that of a harmonic chain as this force is increased. As expected, the general equations of motion (6) and the linear expansion (13) match exactly. We may compactly express the N linear equations in the matrix form

$$\mathbf{M} \frac{d^2 \mathbf{u}}{d\tau^2} = \mathbf{K} \mathbf{u} + \mathbf{f}, \quad (14)$$

where \mathbf{M} is a diagonal matrix with the random mass ratios $b^{(1)}$ through $b^{(N)}$ on the diagonal, and \mathbf{K} is a symmetric, tri-diagonal matrix. The sub- and

superdiagonal elements are given by $\mathbf{K}(i, i - 1) = \kappa_{(i-1,i)}$ and $\mathbf{K}(i, i + 1) = \kappa_{(i+1,i)}$, respectively. The diagonal entries are $\mathbf{K}(i, i) = -(\kappa_{(i-1,i)} + \kappa_{(i+1,i)})$. Since the stiffnesses depend on the contacting particles, these values are random in general. The forcing vector \mathbf{f} has only one non-zero entry, which is $f_1(\tau) = \epsilon \sin \omega_o \tau$ in the first position. Other entries cancel by the equilibrium condition $\kappa_{(i-1,i)} \Delta_{(i-1,i)} = \kappa_{(i+1,i)} \Delta_{(i+1,i)}$.

Since we look to examine the effect of mass disorder alone, we take all coupling stiffnesses to be independent of the contact ($\kappa_{(i,j)} = 1 \forall i, j$). Accordingly, all initial overlaps are equal with $\Delta_{(i,j)} = 1$. With this assumption, the stiffness matrix simplifies, with \mathbf{K} now having entries of -2 on the diagonal and entries of $+1$ on the sub and superdiagonal.

We examine the solutions of the linear system (14) in section 2.2.

2.1.3 Nonlinear Hertzian coupling: $\beta = 1/2$

With $\beta = 1/2$ we obtain the Hertz contact model and the equations of motion are given by (6), (7), and (8). The interparticle forces are dependent on the size and material properties of the constituent particles (see Appendix B). We find that the scaled stiffness $\kappa_{(i,j)}$ and initial overlap $\Delta_{(i,j)}$ are given by

$$\kappa_{(i,j)} = \sqrt{\frac{2}{b^{(i)1/3} + b^{(j)1/3}}} \left(b^{(i)} b^{(j)} \right)^{1/6}, \quad (15)$$

and

$$\Delta_{(i,j)} = \kappa_{(i,j)}^{-2/3}. \quad (16)$$

As in the linearized version of the Hertz chain of given by (14), the nonlinear chain of polydisperse spheres is, in general, disordered in both mass and coupling stiffness.

2.1.4 Creation of mass-disordered, monodisperse chains

If we wish to remove the effects of contact disorder present in the Hertzian model one may consider the modification of particles to create a monodisperse (size) chain of varied mass. In this manner we may isolate the effect of mass disorder. Numerically incorporating such a construction is trivial; the equations of motion are given by (6), (7), and (8) and we assign $\kappa_{(i,j)} = 1$ and $\Delta_{(i,j)} = 1$ for all contacts (i, j) . In an experimental realization, one may imagine creating such a monodisperse, mass-disordered chain by the removal of material from the particle centers or the inclusion of denser cores. Since the Hertz model is based on deformations local to the contacting surfaces, this change of mass should have a negligible effect on the contact stiffnesses provided the modification is sufficiently far from the surface.

2.2 Linear model– Eigenvalue analysis

With the goal of solving for the general motion of the linear chain under the imposed boundary conditions, we look to phrase (14) in its eigenvector basis. This transformation decouples the equations of motion into N independent relations, facilitating the process of finding a general solution. Upon determination of the

solution in the eigensystem, a simple linear transformation yields the motion of the particles.

Thus we first seek to determine the eigenvectors and eigenfrequencies associated with (14). We set $\mathbf{f} = \mathbf{0}$ and assume that for each normal mode all masses oscillate with a particular frequency ω . Defining $\mathbf{A} \equiv -\mathbf{M}^{-1}\mathbf{K}$ (not symmetric, in general) we arrive at the familiar eigenvalue problem:

$$\mathbf{A}\mathbf{u} = \omega^2\mathbf{u}. \quad (17)$$

This may be solved numerically to determine the set of N orthonormal eigenmodes $\{\mathbf{s}_{(j)}\}$ and eigenfrequencies $\{\omega_{(j)}\}$. We normalize the eigenvectors to have the following orthonormality conditions (see Appendix A):

$$\mathbf{s}_{(i)}^T \mathbf{M} \mathbf{s}_{(j)} = \delta_{ij}, \quad (18)$$

where δ_{ij} is the usual Kronecker delta symbol.

We sort the eigenvectors by increasing order of their associated eigenvalues (frequencies) and assemble the $(N \times N)$ matrix \mathbf{S} such that the j^{th} column is eigenvector $\mathbf{s}_{(j)}$. Using \mathbf{S}^{-1} as the transformation matrix between the particle displacements \mathbf{u} and the eigenmode amplitudes \mathbf{z} , we have $\mathbf{z} = \mathbf{S}^{-1}\mathbf{u}$. We also note the similarity transform $\mathbf{S}^{-1}\mathbf{A}\mathbf{S} = \mathbf{D}$, where \mathbf{D} is a diagonal matrix with the (increasing) eigenvalues along the diagonal.

With the use of \mathbf{S} we transform the general equation of motion (14) and obtain the decoupled form:

$$\frac{d^2\mathbf{z}}{d\tau^2} = -\mathbf{D}\mathbf{z} + \mathbf{h}, \quad (19)$$

where $\mathbf{h} = \mathbf{S}^{-1}\mathbf{M}^{-1}\mathbf{f}$. We are thus left to solve N independent equations of the form:

$$\frac{d^2z_j}{d\tau^2} + \omega_{(j)}^2 z_j = h_j, \quad (j = 1, \dots, N). \quad (20)$$

For the case of $h_j = 0$ (*i.e.* no driving) we obtain the trivial harmonic solution $z_j = z_j^{(0)} \exp(\pm i\omega_{(j)}\tau) = A_j \sin \omega_{(j)}\tau + B_j \cos \omega_{(j)}\tau$. In our specific case of harmonic driving, the transformed forcing vector \mathbf{h} may be rephrased as follows. Since $\mathbf{f} = \epsilon \sin \omega_o \tau \mathbf{e}_1$ ($\mathbf{e}_1 = [1 \ 0 \ \dots \ 0]^T$) we have:

$$\mathbf{h} = \mathbf{S}^{-1}\mathbf{M}^{-1}\epsilon \sin \omega_o \tau \mathbf{e}_1 = \frac{\epsilon \sin \omega_o \tau}{b^{(1)}} \mathbf{y} \quad (21)$$

where $\mathbf{y} = \mathbf{S}^{-1}\mathbf{e}_1$ is the first column of \mathbf{S}^{-1} . Exploiting the orthogonality given in (18) we left-multiply \mathbf{y} by $\mathbf{S}^T \mathbf{M} \mathbf{S} = \mathbf{I}$ and find $\mathbf{y} = \mathbf{S}^T \mathbf{M} \mathbf{e}_1 = b^{(1)} \mathbf{S}^T \mathbf{e}_1$. Thus \mathbf{y} is proportional to the first row of \mathbf{S} . We then write (20) as

$$\frac{d^2z_j}{d\tau^2} + \omega_{(j)}^2 z_j = \epsilon S_{1j} \sin \omega_o \tau, \quad (22)$$

which has the general solution

$$z_j(\tau) = A_j \sin \omega_{(j)}\tau + B_j \cos \omega_{(j)}\tau + \frac{\epsilon S_{1j}}{\omega_{(j)}^2 - \omega_o^2} \sin \omega_o \tau. \quad (23)$$

The $2N$ undetermined constants $\{A_j\}$ and $\{B_j\}$ are determined from the initial conditions $\mathbf{z}(0) = \mathbf{S}^{-1}\mathbf{u}(0)$. Taking $\mathbf{u}(0) = \mathbf{0}$ and $d\mathbf{u}/d\tau(0) = \mathbf{0}$ as the initial conditions on particle displacements and speeds, we have:

$$z_j(\tau) = \frac{\epsilon S_{1j}}{\left(\omega_{(j)}^2 - \omega_o^2\right)} \left(\sin \omega_o \tau - \frac{\omega_o}{\omega_{(j)}} \sin \omega_{(j)} \tau \right), \quad (24)$$

which transforms back to the expression for the displacement history of particle p ,

$$u^{(p)}(\tau) = \sum_{j=1}^N S_{pj} z_j(\tau) = \epsilon \sum_{j=1}^N \frac{S_{pj} S_{1j}}{\left(\omega_{(j)}^2 - \omega_o^2\right)} \left(\sin \omega_o \tau - \frac{\omega_o}{\omega_{(j)}} \sin \omega_{(j)} \tau \right). \quad (25)$$

For a given chain arrangement, we may calculate the displacement history from (25) and this way investigate the frequency spectrum at a particular location in the chain. Discussion of the terms in (25) is deferred to section 3.3.

We finally note that in the case of an undriven ($\epsilon = 0$) monodisperse linear chain, we obtain the dispersion relation [1],

$$\omega(k) = 2 \sin k r_o, \quad (26)$$

where k and r_o are the dimensionless wavenumber (purely real) and particle radius, respectively. This sets the cutoff frequency for propagative waves at $\omega \leq \omega_{max} = 2$. At $\omega_{max} = 2.0$ we have the minimum wavelength $\lambda_{min} = 4r_o$. That is, signal frequency components in the pass-band of $0 < \omega \leq 2$ propagate without attenuation. Frequencies above the cutoff are termed evanescent waves as the wavenumber has an imaginary component which causes the signal to exponentially decay with distance. Since our random chains contain masses distributed about the monodisperse system of $b^{(i)} = 1$ we will consider driving frequencies ω_o on the order of $\omega = 2$, in the range $[0.1\omega_{max}, 1.6\omega_{max}]$.

3 Results and Discussion

In this section we present results on the high-frequency filtering effects of random chains.

Section 3.1 discusses the construction of the random systems for several mass distributions. We also introduce our definition of the disorder parameter.

Section 3.2.1 contains results for the chain with linear contact forces, with masses chosen from a normal mass distribution and uniform contact stiffness, examining the effects of disorder and driving frequency. A comparison of mass distributions is shown in 3.2.2, and section 3.2.3 investigates the role of coupling (contact stiffness) disorder in harmonic chains.

Results related to the nonlinear chain are presented in section 3.4. Similar to the linear chain we perform a parameter study in section 3.4.1 and examine the effect of disorder and driving frequency. The driving amplitude is also considered. We follow this in section 3.4.2 with results for the nonlinear chain featuring uniform contact interactions, which isolates the effect of mass disorder.

3.1 Chain generation

We introduce mass disorder to the chains by employing random number algorithms that approximate a specified probability distribution. In this study we consider normal $f^{(n)}(b)$, uniform $f^{(u)}(b)$, and binary discrete $f^{(d)}(b)$ distributions, where b is the scaled mass.

For the normal distribution, we prescribe the mean μ and standard deviation $\sigma = \xi\mu$. Due to the scaling by the mean mass, $\mu = 1$ and $\sigma = \xi$. The parameter ξ determining the magnitude of the standard deviation will be used to quantify the disorder of the system. When sampling masses to create the normally distributed random chains, we enforce a lower cutoff such that $b_{min} > 0$. No such cutoff is implemented for the largest masses. In Figure 1 we plot the ensemble-averaged $\langle b_{min} \rangle$ and $\langle b_{max} \rangle$. For each figure we average over a set of 10^5 chains sampled from a normal distribution (mean $\mu = 1$ and standard deviation ξ), with each chain containing 2000 particles. We note that the restriction of $b > 0$ causes the ensemble-averaged minimum mass values to be bounded as we increase the width of the distribution (disorder) ξ . Values of the largest ensemble-averaged masses increase linearly with ξ , as expected.

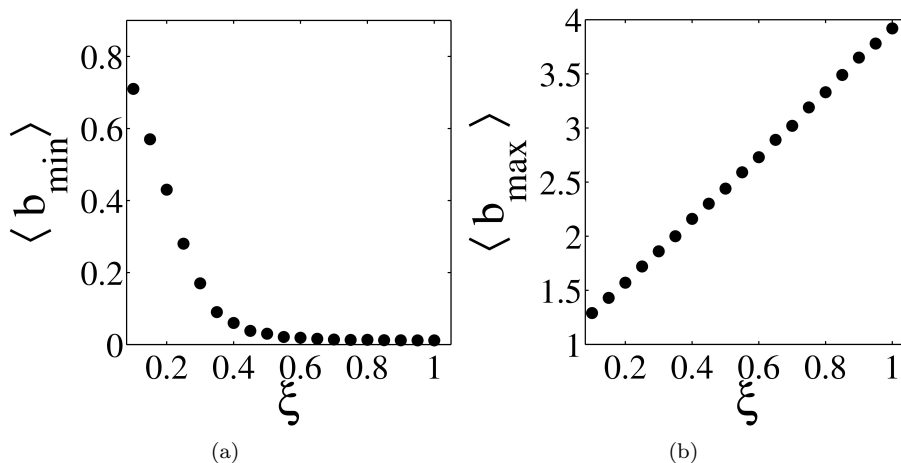


Figure 1: Ensemble-averaged minimum and maximum masses. The masses are sampled from normal distribution with mean $\mu = 1$ and standard deviation ξ . Each chain contains 2000 particles and the ensemble has 10^5 chains.

For comparison between the three distributions, we match the moments of the theoretical probability density functions. In general, the n^{th} moment of a given distribution $f^{(q)}(b)$ is defined as,

$$M_n^{(q)} = \int_{-\infty}^{\infty} b^n f^{(q)}(b) db, \quad (27)$$

where q is used to identify the specific distribution type. Since only positive masses are permitted, the lower limit of integration may be changed to zero.

For probability distributions, the zeroth moment is 1 by definition. A normal distribution with mean $\mu = 1$ and standard deviation $\sigma = \xi$ has $M_1^{(n)} = 1$,

$M_2^{(n)} = 1 + \xi^2$. The uniform distribution in the interval $[b_a, b_b]$ (symmetric about $\mu = 1$) has $M_1^{(u)} = (b_b + b_a)/2$ and $M_2^{(u)} = (b_b^2 + b_a b_b + b_a^2)/3$. Equating $M_1^{(n)} = M_1^{(u)}$ and $M_2^{(n)} = M_2^{(u)}$ we obtain:

$$b_a = 1 - \sqrt{3}\xi, \quad (28)$$

$$b_b = 1 + \sqrt{3}\xi. \quad (29)$$

The binary discrete distribution with masses b_c and b_d is given by $f^{(d)}(b) = c_1\delta(b - b_c) + (1 - c_1)\delta(b - b_d)$, where $\delta(s)$ is the Dirac-delta function. The n^{th} moment is $M_n^{(d)} = c_1 b_c^n + (1 - c_1)b_d^n$. Matching the first *three* moments to that of the normal distribution we find,

$$b_c = 1 - \xi, \quad (30)$$

$$b_d = 1 + \xi. \quad (31)$$

Note that in matching the moments of the distributions, the requirement that $b_a > 0$ (non-zero, positive mass) in (28) imposes that $\xi < 1/\sqrt{3} \approx 0.5774$.

By employing three different mass distributions that have the same moments, we may compare the filtering behavior of these systems and investigate the role that the mass distribution plays.

3.2 Linear chain filtering

Given an array of $(N + 2)$ random masses (where the end particles have prescribed motion), we numerically solve the eigenvalue problem as described in section 2.2, yielding the $(N \times N)$ eigenvector matrix \mathbf{S} and the N eigenfrequencies $\{\omega_{(j)}\}$ ($j = 1, \dots, N$). With equation (25) we calculate the displacement history $u^{(p)}(\tau_n)$ of particle p at discrete time steps $\tau_n = n\tau$ on the interval $\tau = [0, \tau_{max}]$. The time window is sufficiently large and the scaled time step $d\tau$ is chosen to be small enough to permit sampling at the frequencies of interest. We then perform a discrete Fourier transform to obtain the spectrum of this signal. In particular, we examine the absolute value of the Fourier components, $U^{(p)}(\omega)$. This calculation is performed for particles $p = 1, \dots, M$. The length of the chain $(N + 2)$, M , and τ_{max} are chosen such that the signal has not reflected from the fixed particle $p = N + 1$ and the high frequencies have been given sufficient time to propagate due to their lower phase velocity. The spectra of oscillations for the sampled particles may be compactly visualized by the use of a three-dimensional plot projected into a two-dimensional plane. Here we plot in the (p, ω) plane and represent the values of the absolute Fourier components $U^{(p)}(\omega)$ with a greyscale. At each location p , the $U^{(p)}(\omega)$ array of values is normalized to unity. In our convention, darker shades correspond to larger values with the scaling set such that black corresponds to a Fourier component ≥ 0.2 . This is applied for all of the following figures. For two particular chain arrangements, we obtain Figure 2. We will later show averages over 200 different realizations.

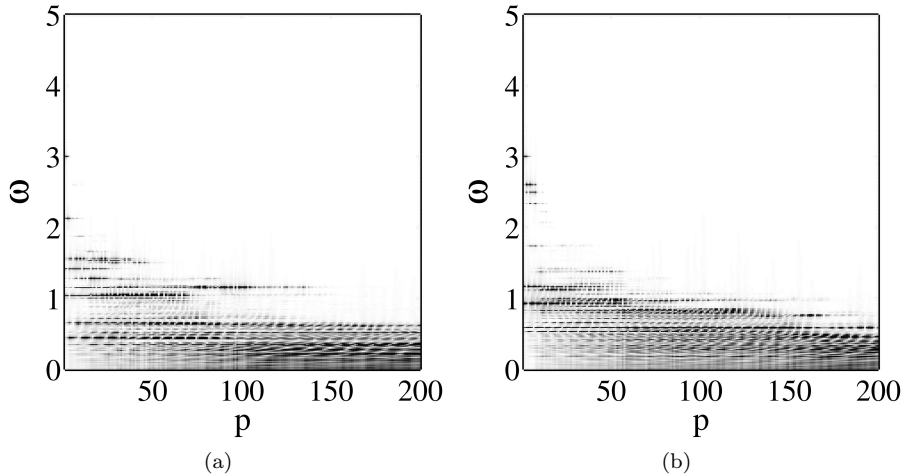


Figure 2: Frequency propagation spectrum for two instances of a single realization of a normally distributed disordered chain with uniform linear coupling. $\xi = 0.5$, $\omega_o = 3$, $d\tau = 0.0667$, $\tau_{max} = 546.41$, $N = 500$, $M = 200$.

In both of Figures 2a and 2b we note a rapid decrease of the input frequency within several particle diameters from the driver. Following this, we observe the persistence of several lower frequencies ($\omega < \omega_o$) which are dependent on the particular chain arrangement. However, by $p = 200$ we note that the frequency content of the two arrangements is more comparable and frequencies $\omega \gtrsim 0.5$ have absolute Fourier components that are relatively small with respect to $\omega \lesssim 0.5$. This range of propagated frequencies is dependent on the disorder parameter, as investigated in Section 3.2.1.

Examining the evolution of a particular frequency component ω^* as it propagates down the chain, we note the dark and light oscillations (“stitching”) apparent for certain frequencies in both plots of Figure 2. For lower frequencies, the wavelengths of these features match closely with those obtained from the dispersion relation (26) for the perfect chain, as shown in Figure 3. Here, for a single chain realization, we compare the features of the dispersion relation to the spatial filtering behavior. To construct this figure we perform a discrete double Fourier transform of the $u^{(p)}(\tau)$ signal. With this plot we may examine the wavelength λ of the stitching as ω^* is varied. Note the close agreement between the analytical result (black circles) and the data in the low-frequency/long-wavelength limit ($\omega \lesssim 0.5$). As the frequency increases, there is significant deviation of the disordered system from the monodisperse chain. The dark horizontal lines change with the particular chain arrangement and correspond to strong, but spatially short excitations, indicating localization of the oscillations at frequency ω^* .

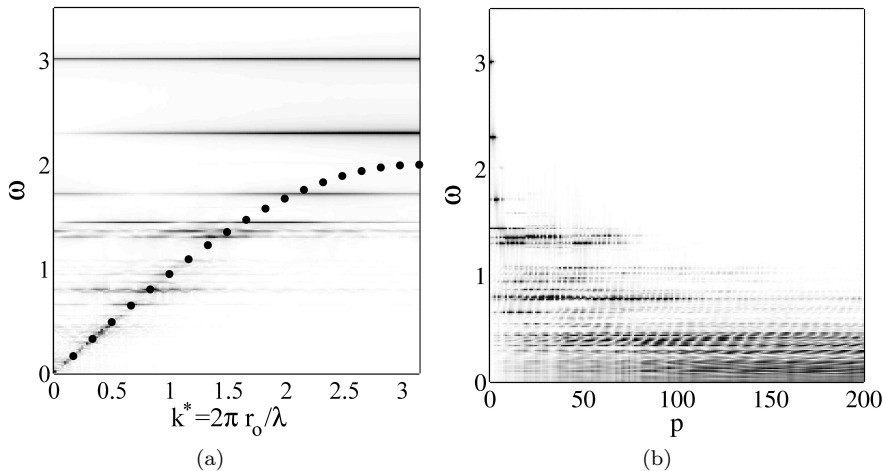


Figure 3: The dispersion relation (a) obtained from the simulation displayed in (b). The black circles are obtained from the perfect chain dispersion relation (26) at 20 equidistant k^* values. Darker shades correspond to greater magnitude Fourier components.

The light areas of the stitching thus correspond to nodes of the wave, where the oscillations at the particular frequency ω^* are insignificant. Based upon the chain arrangement this behavior is more visually apparent at certain frequencies, but Figure 3 confirms that there is a “selected” wavelength associated with the oscillations at each frequency. However, we note that the stitching is a consequence of the wave component interactions since it is not present in our simulations with perfect chains; in such cases a monochromatic horizontal line is observed to propagate without change (if $\omega \leq 2$). Simulations of perfect chains produce dispersion plots that exactly match the black circles plotted in Figure 3.

3.2.1 Frequency-filtering of the monodisperse linear chain: normally distributed masses

Here we employ a normal distribution of masses and perform a parameter study on the effects of disorder magnitude ξ and source frequency ω_o . For each set of data, we generate an ensemble of 200 random chains. Each chain contains $N = 500$ particles and we examine the displacement signal for particles 1 through $M = 200$. Selection of the chain length N and the value of M is based on examining the results of longer systems; for relatively high disorder ($\xi = 0.5$) we note minimal change in the spectrum of transmitted frequencies beyond approximately 200 particles from the excitation source.

By requiring that the signal does not reach the fixed end-particle $p = (N+1)$, a sampling time interval $\tau = [0, \tau_{max}]$ is approximately determined from the analysis of several chain arrangements (“microstates”). If the fixed end is indeed reached in a particular microstate, the reflected signal certainly does not have sufficient time to propagate backwards to the specified sampling region, $p < M$.

With τ_{max} set, we divide the time span into q steps such that $d\tau = \tau_{max}/q$ is small enough to detect the relevant large frequencies in a given signal. As

stated in Section 2.2, a monodisperse linear chain will propagate normalized frequencies $\omega \leq 2$ and we drive the disordered chains at frequencies of this order. We select $q = 8192$ time steps which yields $d\tau \approx 0.0667$ for the given time interval. We note that this time step permits detection of frequencies $\omega \lesssim 47.1$, which is many times greater than the largest eigenfrequencies.

For each realization in the ensemble of disordered chains, we calculate the motion and the Fourier transform for the particles in the sampled region $p < M$. To obtain the ensemble frequency content, we subsequently average over the Fourier transform data for each microstate.

We emphasize that for Sections 3.2.1 through 3.2.2 we are concerned with systems where only the masses are disordered. The coupling stiffnesses $\kappa_{(ij)} = 1$ are the same for all contacts in the chain. In section 3.2.3 we vary the contact stiffnesses along with the particle masses.

Fix ω_o , vary ξ : Here we set the driving frequency $\omega_o = 3.0$ to a constant value and vary the disorder parameter ξ as shown in Figure 4. In this manner we may examine the effect of disorder on the transmitted frequencies. We note that the greyscale values for each subplot are the same, with the absolute Fourier component of magnitude 0 corresponding to white and 0.2 or greater appearing black.

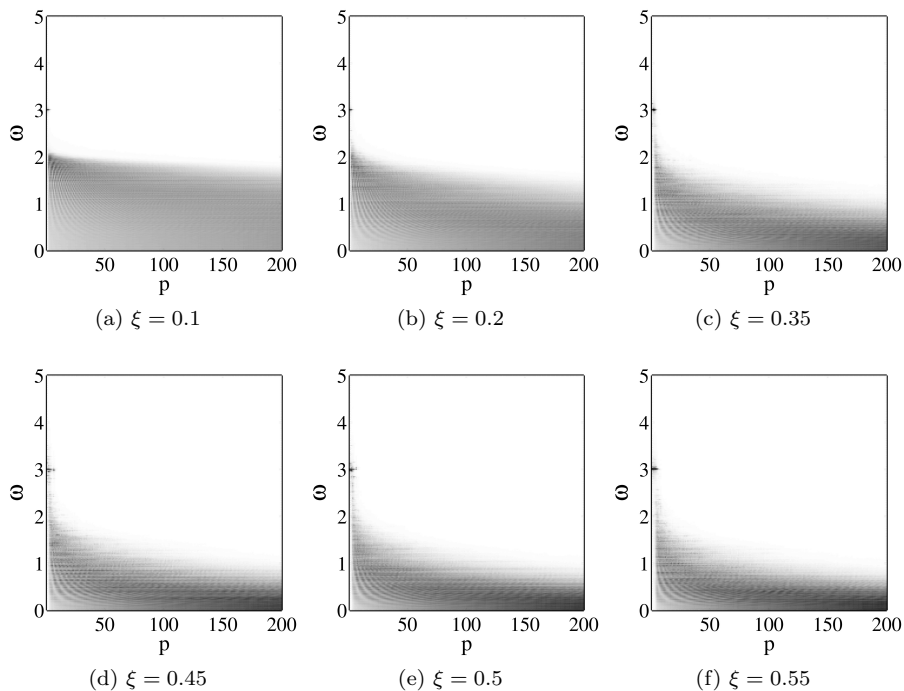


Figure 4: Variation of the disorder parameter ξ . The source frequency $\omega_o = 3.0$ and the other parameters are the same as in Figure 2.

From Figure 4 we note that as the disorder parameter increases (from subfigures 4a to 4f) there is an associated decrease in the transmission of the relatively higher frequency components. For select disorder values, we plot the ensemble-averaged spectrum of particle $p = 200$, $\langle U^{(200)}(\omega) \rangle$, in Figure 5.

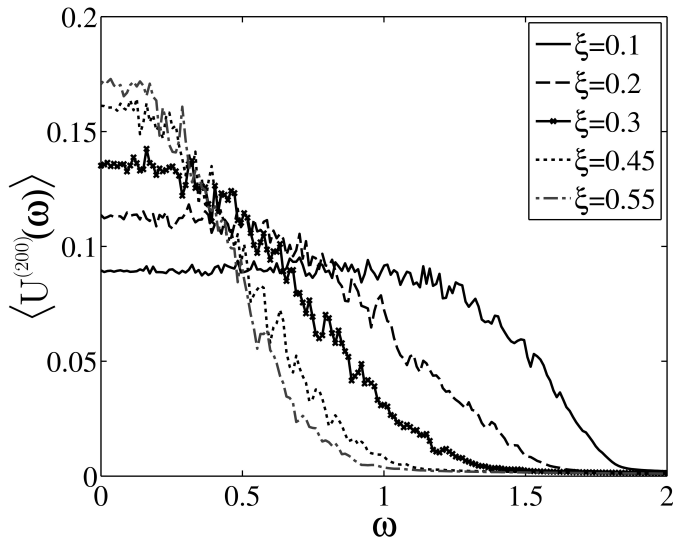


Figure 5: Ensemble-averaged spectrum at the 200th particle for various levels of disorder, from the data in Figure 4. For clarity, we omit data from several disorder magnitudes.

From Figure 5 we see that increased disorder leads to decreased magnitude of the higher frequency components, as observed in Figure 4. Note that the perfect (monodisperse) chain excited at $\omega_o = 3.0$ would have a profile that is flat for $0 \leq \omega \leq 2$ followed by a sharp cutoff to zero for $\omega > 2$. As the disorder increases towards $\xi = 0.55$, the profiles of the transmitted frequency spectrums begin to converge. Increase of ξ beyond $1/\sqrt{3}$ (although not permitted for comparison of the mass distributions as explained in Section 3.1) reveals little difference in the profile of transmitted frequencies. This suggests that the system disorder may be saturated and a further increase of the disorder parameter does not significantly affect the ensemble-averaged signal transmission properties.

In Figure 6 we plot the density of states for various values of the disordered parameter. The eigenvalues for 2000 states of a 500 particle chain are numerically calculated and the density of states is normalized such that the sum of values (for each ξ) is unity. The numerical results are plotted with the analytical result for a perfect chain as given by Sheng [37],

$$\rho(\omega) \sim \frac{1}{\sqrt{4 - \omega^2}} \quad (32)$$

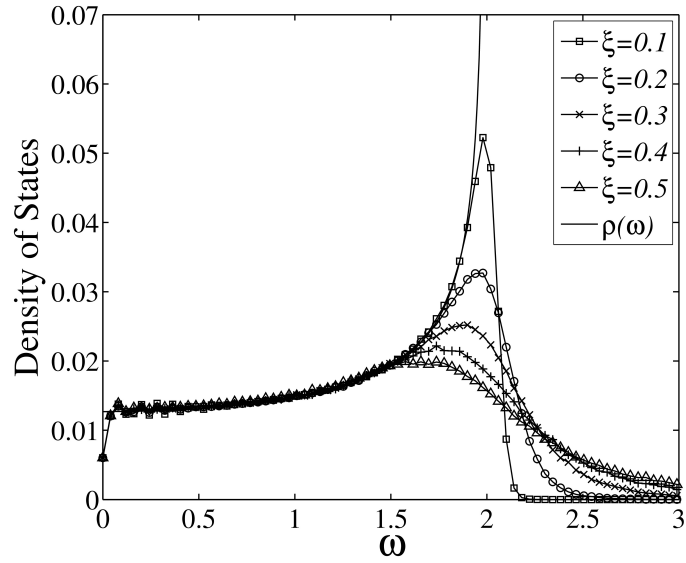


Figure 6: Density of states for mass-disordered chains. The curve $\rho(\omega)$ is the analytical result (32) for the density of states in a monodisperse chain.

In Figure 6 the density of states generally increases as we approach the cutoff frequency $\omega = 2.0$ of the ordered chain. As the disorder increases, the introduction of more smaller masses permits higher frequency oscillations and the density of states accordingly increases for the greater frequencies. From Figure 2 we see some limited transmission of frequencies $\omega > 2.0$, which is not observed in the perfect chain with zero density of states for $\omega > 2.0$.

Fix ξ , vary ω_o : Here we set the disorder parameter at a constant $\xi = 0.3$ and vary the source frequency ω_o . For each driving frequency we employ the same ensemble of 200 normally-distributed random mass chains. Greyscale is individually adjusted for visualization of each subplot. Results for six input frequencies are shown in Figure 7.

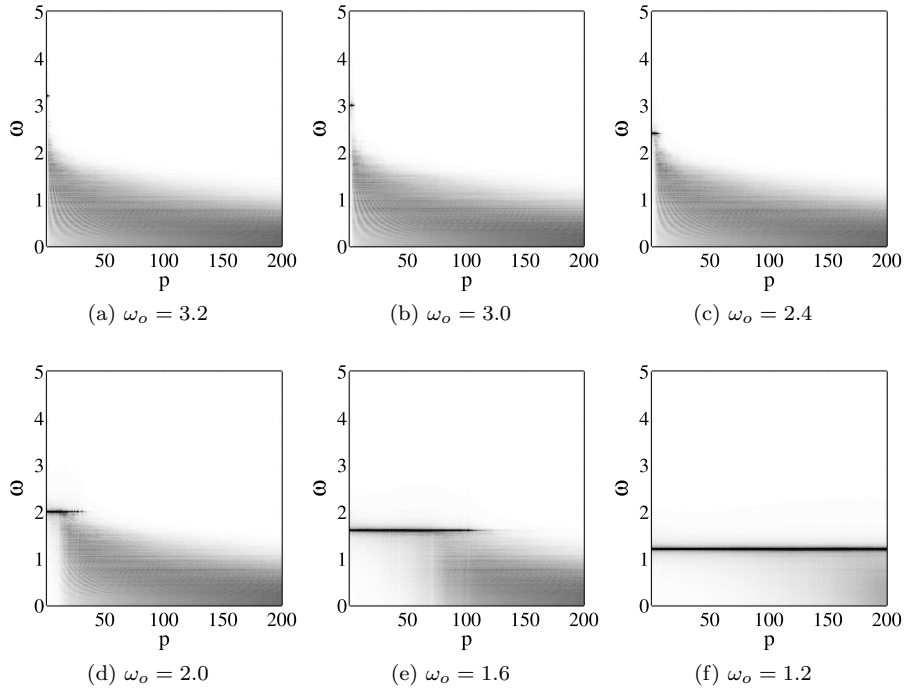


Figure 7: Variation of the source frequency ω_o , for disorder parameter $\xi = 0.3$ and other parameters as in Figure 2.

As suggested by the plots of Figure 4, lower frequency signal components are not as affected by the presence of mass-disorder. This is clearly shown in Figure 7 where the frequency components corresponding to the excitation are shown to propagate further into the system for decreasing ω_o . As evidenced by Figure 6 low frequency (long wavelength) oscillations of disordered arrangements capture the dispersion behavior of ordered systems and thus low frequency inputs propagate as in perfect chains. Qualitatively similar results are obtained for other values of the disorder parameter ξ .

3.2.2 Frequency-filtering of the linear chain: comparison of mass distributions

Here we compare the results for different mass distributions. As detailed in Section 3.1 we employ normal, uniform, and binary distributions such that the moments are matched for a given disorder parameter ξ . In each row of Figure 8 we plot the results for a given distribution. By looking at individual columns, we may compare the results for the various distributions. Aside from small discrepancies close to the source (subfigures 8c, 8f, 8i) we note that the spectrum of transmitted frequencies are the same for the three mass distributions studied at all disorder measures. Plotting the frequency spectrum at $p = 200$ reveals no significant difference between the three mass distributions.

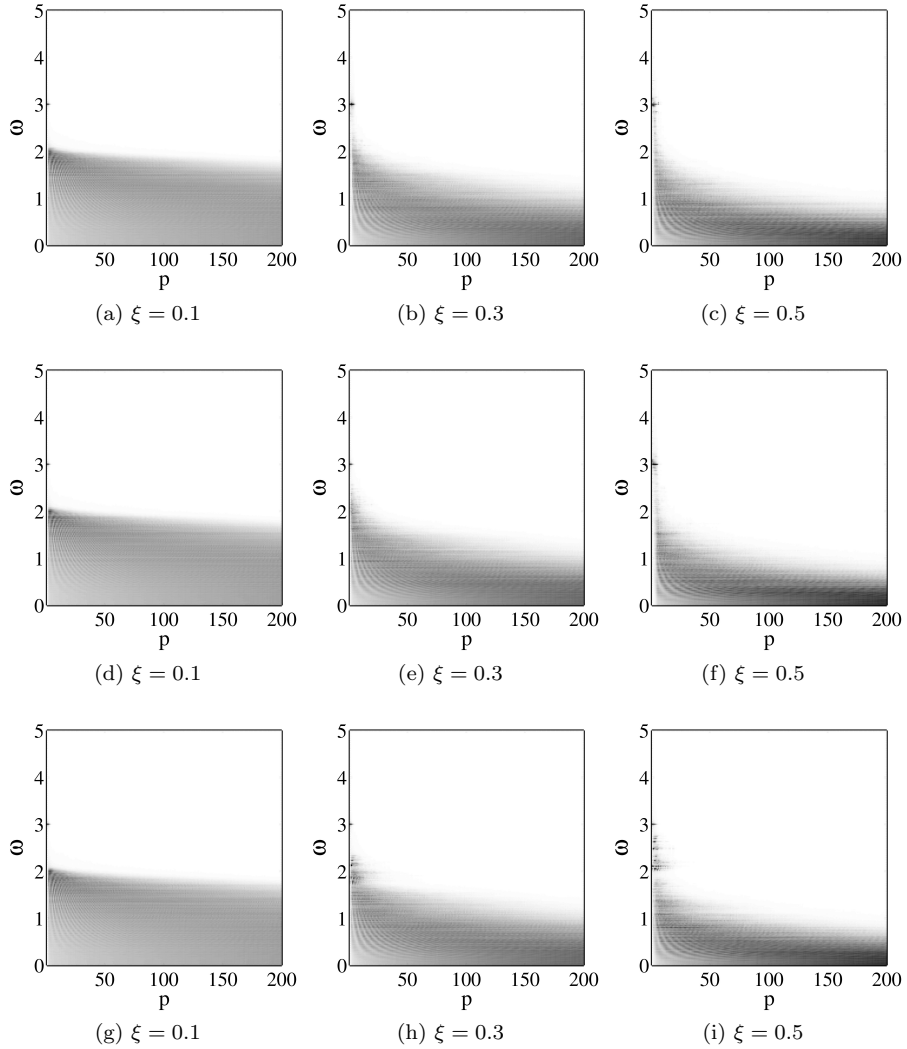


Figure 8: Comparison of normal [(a), (b), (c)], uniform [(d), (e), (f)], and binary mass distributions [(g), (h), (i)] for $\xi = 0.1, 0.3, 0.5$

The quantitative similarity of the transmission profiles for the binary mass system (as compared to the normal and uniformly distributed systems) suggests that the intermediate mass particles do not have a significant effect on the bulk filtering properties of the disordered systems. The relevant measure of disorder is indeed related to the moments of the mass distribution.

Equation (4) with $\beta = 0$ shows that the characteristic (dimensional) time scale is $\tilde{t}_c = \sqrt{\tilde{m}_o/\tilde{\kappa}_o}$. For a monodisperse linear (harmonic) system with masses \tilde{m}_o and spring stiffness $\tilde{\kappa}_o = \tilde{k}_n$, we may identify the natural frequency $\tilde{\omega}_n = 1/\tilde{t}_c = \sqrt{\tilde{k}_n/\tilde{m}_o}$. From Section 2.2 we recall that monodisperse chains transmit frequencies in the passband $\omega = \tilde{\omega}/\tilde{\omega}_n \leq 2.0$. Thus, monodisperse chains of relatively larger masses will accordingly transmit lower frequencies. Although we are concerned with disordered systems, one may argue that it is the largest masses present in the disordered chains that inhibit the propagation of relatively high frequencies. The inclusion of a small amount of relatively large masses in monodisperse chains of small masses shows a similar low-pass filter behavior.

3.2.3 Frequency-filtering of the mass- and contact-disordered linear chain

Here we present results for the linearized approximation to the general nonlinear governing equations (equation (13) with $\beta = 0$). This is equivalent to a linear chain where the mass and contact stiffness are both disordered. The non-dimensional contact stiffness is related to the sizes of the contacting particles as given in (15). Comparison of Figures 9a–9c with the corresponding plots

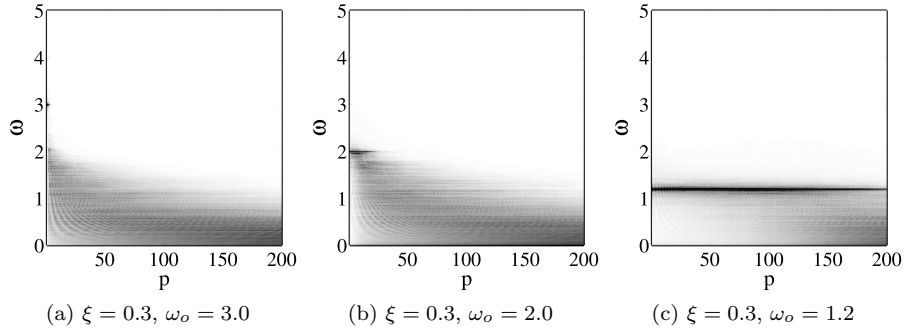


Figure 9: Mass- and contact-disordered chain for $\xi = 0.3$ and $\omega = 3.0, 2.0, 1.2$

of Figure 7 reveals that the addition of contact disorder leads to a more rapid spatial decay of the input frequency ω_o . We also note that the bandwidth of transmitted frequencies is marginally reduced for the contact-disordered chains, as evidenced by plotting the profiles at various downstream locations (plots not shown). However, the shape of the profiles are qualitatively comparable.

3.3 Disorder and localization

From Section 2.2 we recall that the displacement history of particle p is given by (25):

$$u^{(p)}(\tau) = \epsilon \sum_{j=1}^N \frac{S_{pj}S_{1j}}{\left(\omega_{(j)}^2 - \omega_o^2\right)} \left(\sin \omega_o \tau - \frac{\omega_o}{\omega_{(j)}} \sin \omega_{(j)} \tau \right). \quad (33)$$

We examine the $S_{pj}S_{1j}$ term present in the numerator of expression (33). Recall that the matrix \mathbf{S} is constructed such that the j^{th} column is the scaled j^{th} eigenvector, sorted in increasing order of the associated eigenvalues. Thus, each column represents a mode shape and the entry S_{pj} is the (scaled) displacement of particle p in mode j . $S_{pj}S_{1j}$ is then the product of the displacements of particles p and 1 in mode j .

In the case of the monodisperse linear chain, the eigenvectors are sinusoids subject to the condition that the end particles remain fixed. This imposes the requirement that the eigenmode wavelengths are scalar multiples of π/L , where L is the chain length. For the disordered chain, we note that eigenmodes of increasing frequency exhibit mode localization. This so-called ‘‘Anderson’’ localization has been observed in many physical contexts including mechanical systems of vibrating masses [20,33]. In Figure 10 we plot selected mode shapes of three random chains. The low frequency modes (*e.g.*, Figures 10a and 10b) are similarly shaped for the different chains and are ‘‘extended’’ in nature—the displacements are not localized about a portion of the chain as seen in the higher frequency modes (10c to 10f). In addition to the increased localization of higher frequency modes, we note that the displacements are located at different positions in the chain, indicating sensitivity to the particular mass arrangement. The highest frequency modes approach Dirac–delta functions where only a single particle has a significant displacement (Figure 10f). Physically, the highest frequency modes correspond to smaller mass particles oscillating between two large neighbors.

To quantify the effect of the random mass arrangements on the eigenmodes, we generate a N_e –member ensemble of chains ($N + 2$ particles) and calculate a correlation measure for the set of associated eigenvectors. For each chain we construct the $N \times N$ matrix $\mathbf{S}^{(k)}$ as described prior, with the j^{th} eigenvector $\mathbf{s}_{(j)}^{(k)}$ located in the j^{th} column. The index $k = 1, \dots, N_e$ denotes which microstate of the ensemble is in consideration. We compare two eigenvectors $\mathbf{s}_{(j)}^{(k)}$ and $\mathbf{s}_{(j)}^{(q)}$ through the use of a signed correlation coefficient [18],

$$\text{corr} \left(\mathbf{s}_{(j)}^{(k)}, \mathbf{s}_{(j)}^{(q)} \right) = \frac{\sum_{i=1}^N \left(S_{ij}^{(k)} - \bar{s}_{(j)}^{(k)} \right) \left(S_{ji}^{(q)} - \bar{s}_{(j)}^{(q)} \right)}{(N - 1)\sigma_k\sigma_q}, \quad (34)$$

where the overbar denotes a mean and σ_r is the standard deviation of the components of $\mathbf{s}_{(j)}^{(r)}$. Absolute values of the correlation coefficient range from zero to one, with values close to unity signifying eigenvectors that are highly correlated (such as those of Figure 10a or 10b). Comparing each of the eigenvectors in the N_e –member set leads to $N_e(N_e - 1)/2$ correlation coefficients. The absolute values of these coefficients are averaged to obtain a mode correlation for the

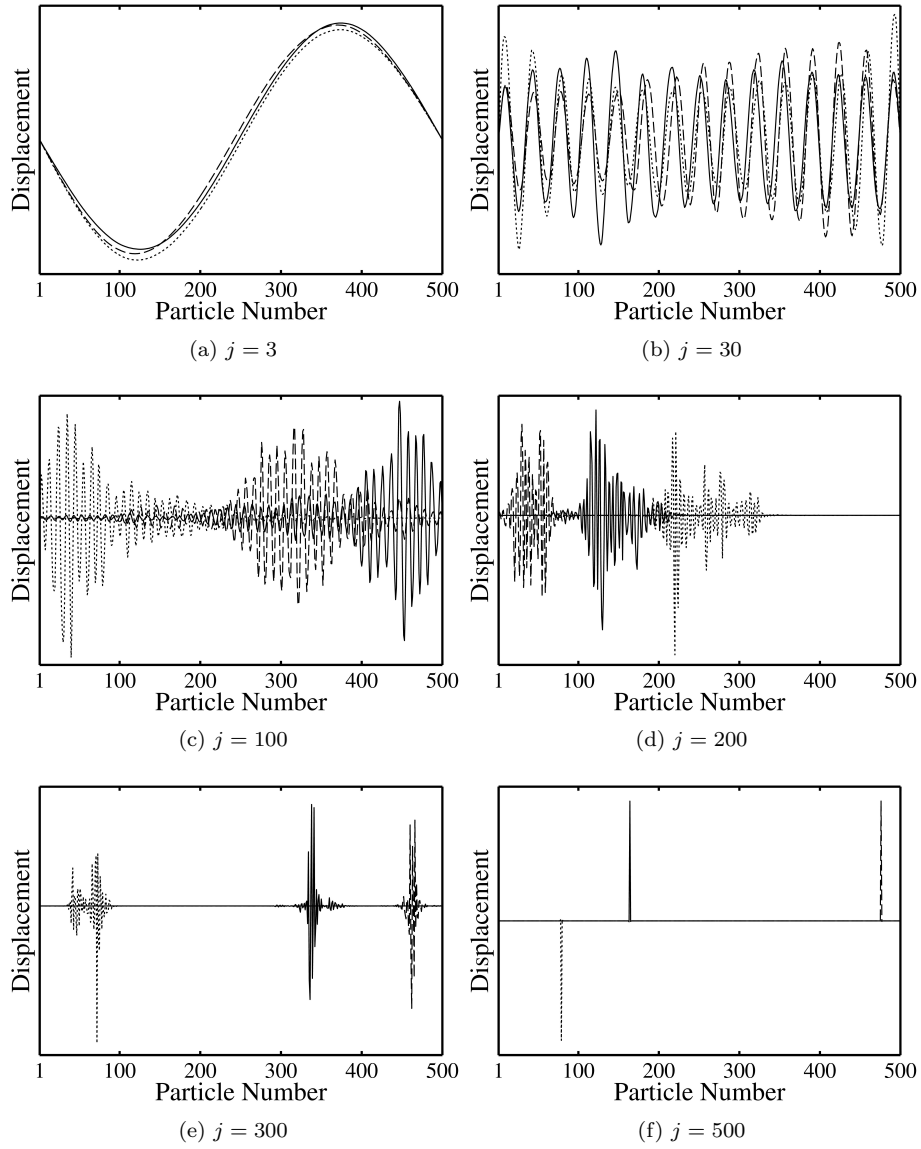


Figure 10: Eigenmode shapes for modes $j = 3, 30, 100, 200, 300, 500$. Each subfigure displays the mode shape for three different random chain arrangements with disorder parameter $\xi = 0.5$.

entire ensemble. We plot this ensemble average correlation $\langle |\text{corr}(\mathbf{s}_j^{(k)}, \mathbf{s}_j^{(q)})| \rangle$ against j in Figure 11:

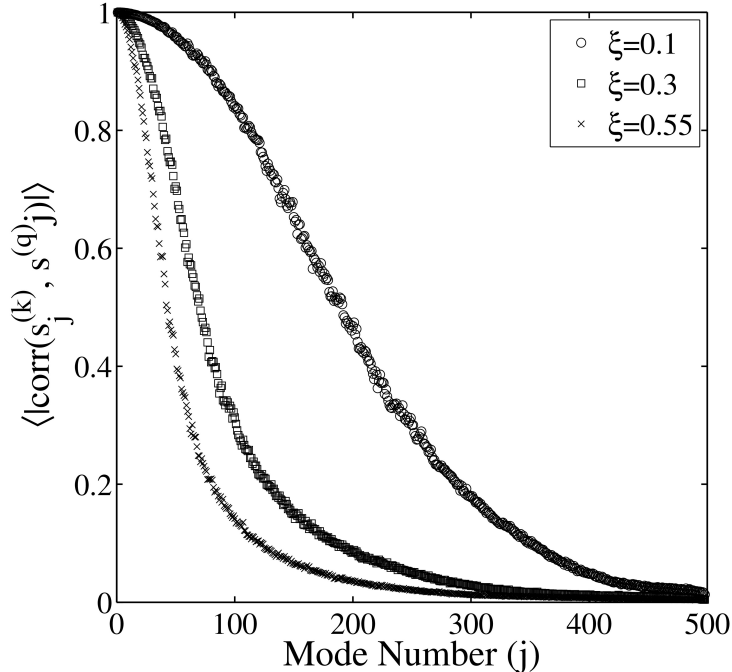


Figure 11: $\langle |\text{corr}(\mathbf{s}_j^{(k)}, \mathbf{s}_j^{(q)})| \rangle$ plotted against the mode number (j). Higher mode number means higher frequency. Results are presented for a 500 particle chain arranged in 200 states. Three disorder values $\xi = 0.1, 0.3, 0.55$ are used.

Further increase of the disorder parameter ξ reveals negligible difference from the case of $\xi = 0.55$, as noted in Section 3.2.1. Since the low-frequency modes remain similar for the various disordered system configurations, we expect similar signal transmission properties for the low-frequency components of an input signal. As shown previously, driving inputs ω_o at relatively low frequencies are less sensitive to the disorder and the input frequency propagates down the chain. Conversely, the uncorrelated nature of the high-frequency modes implies that high-frequency inputs will behave differently in each case, depending on the particular arrangement of masses.

3.4 Frequency-filtering of the nonlinear chain

Similar to the linear chain, in Section 3.4.1 we perform a parameter study of ξ and ω_o for a system of normally-distributed masses with Hertzian interaction. Due to the nonlinearity in the contact law, we also consider the driving amplitude ϵ . We note that the nonlinear chain is, in general, disordered in both mass and contact properties. In Section 3.4.2 we investigate nonlinear chains with uniform contact coupling, isolating the effect of mass-disorder.

3.4.1 Frequency-filtering of the nonlinear chain: normally distributed masses

Fix ω_o , vary ξ : Here we set the driving frequency $\omega_o = 3.0$ and vary the disorder parameter ξ . Three values of ξ are plotted in Figure 12.

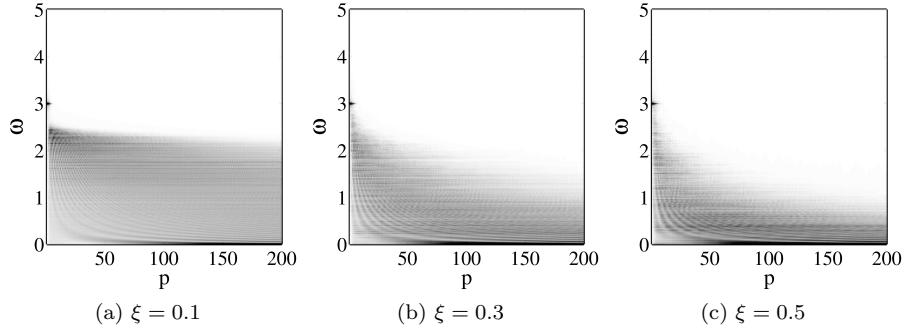


Figure 12: Variation of disorder parameter ξ . Source frequency is $\omega_o = 3.0$ and $\epsilon = 0.05$.

We may compare this with the results of 3.2.3, where a linear contact model is employed for the mass- and contact-disordered chain. As observed in the linear system, increased disorder leads to increased filtering of the high-frequency components. However, the profiles of transmitted frequencies are qualitatively different for the nonlinear chain. In Figure 13 we plot the transmission profiles for particle $p = 200$ for a general nonlinear (with contact-disorder), a contact-ordered nonlinear (see Section 3.4.2), and a contact-disordered linear chain (Section 3.2.3).

We observe that the profiles for the nonlinear chains display a sharp peak at the low frequencies, while the linear chain exhibits a flat profile. The magnitudes of the intermediate frequency components are accordingly less in the nonlinear chain. However, we note that by changing ϵ the oscillation amplitudes will decrease such that we approach behavior that is captured by the linearized model. This is examined in a later section.

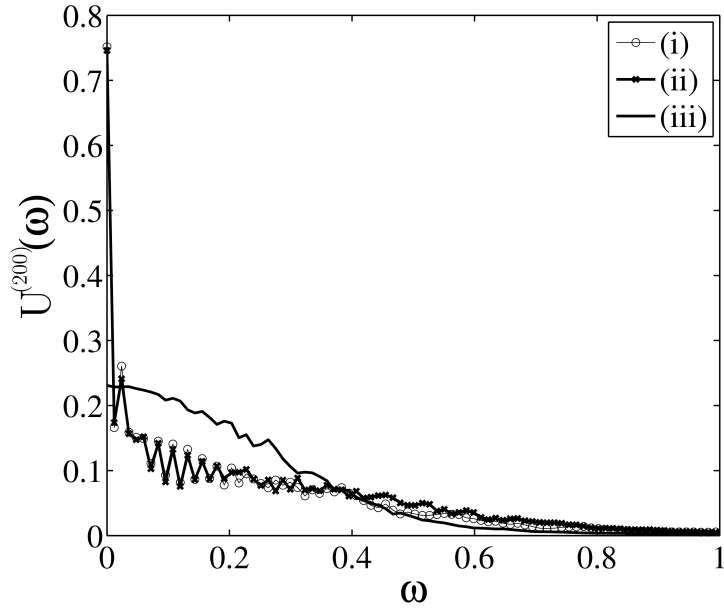


Figure 13: Frequency spectrum at particle $p = 200$ for contact-disordered nonlinear (i), contact-ordered nonlinear (ii), and contact-disordered linear chain (iii). Parameters are $\xi = 0.5$, $\omega_o = 3.0$ and $\epsilon = 0.05$ for the nonlinear chains.

Fix ξ , vary ω_o Here we set the disorder parameter to $\xi = 0.5$ and change the driving frequency ω_o . Results are plotted in Figure 14.

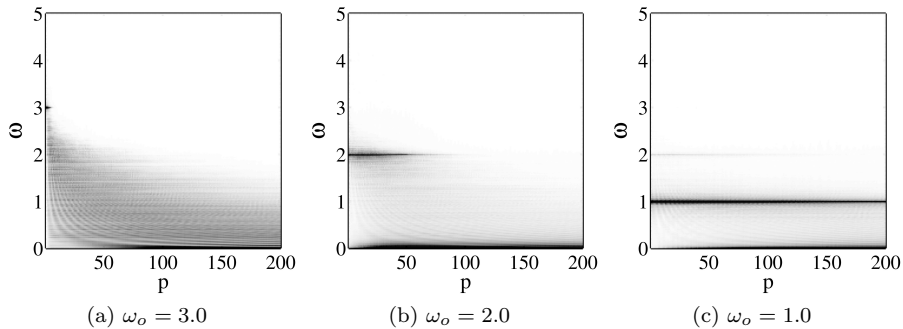


Figure 14: Variation of source frequency ω_o . Disorder parameter is $\xi = 0.3$ and $\epsilon = 0.05$.

As in the linear chain we see that lower frequency signals are not as sensitive to the disorder of the chain and the input frequency propagates further into the system. In Figure 14c we note the appearance of harmonic at $\omega = 2\omega_o$. This frequency doubling harmonic (among others not visible due to the greyscale selection) is a general feature of nonlinear oscillations and is observed in all the simulations. Again we see that the nonlinear chain with an appropriately large excitation ($\epsilon = 0.05$ in this figure) experiences a sharp profile for $\omega \ll 1$.

Driving amplitude Here, the value of the non-dimensional driving amplitude ϵ is varied over several orders of magnitude: $\epsilon = 0.1, 0.05, 5 \times 10^{-3}, 5 \times 10^{-4}$. As noted in (9), the non-dimensional value of ϵ measures the strength of the agitation provided by the driving with respect to the compressive external force on the chain. Thus, small values of ϵ correspond to systems with small driving and/or large confining stress. The largest driving amplitudes are set by the requirement that no contacts may open in the chain, giving ϵ_{max} to be on the order of the characteristic overlap length scale. Simulations check this contact condition to avoid the nonlinearities associated with transient interactions. Results are plotted in Figure 15.

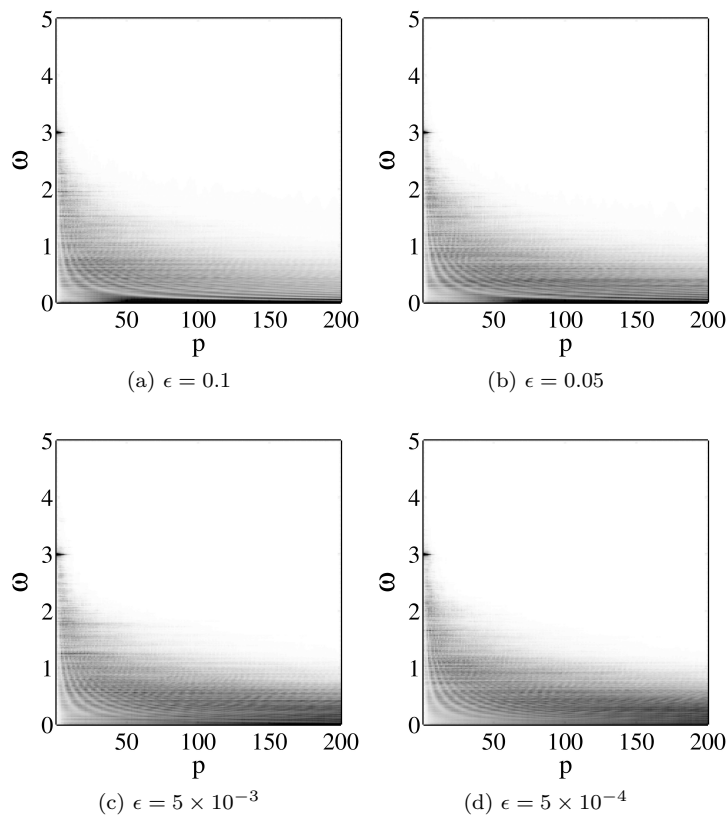


Figure 15: Variation of driving amplitude ϵ . Source frequency is $\omega_o = 3.0$ and $\xi = 0.5$.

Plotting the frequency spectrum at particle $p = 200$ in Figure 16 we note that by decreasing the driving amplitude ϵ we decrease the magnitude of the lowest frequency components. The profiles appear more like that of the linear chain (curve (iii) in Figure 13), consistent with the linearization performed about the equilibrium positions. The approach of a compressed granular system to linear acoustic behavior was noted experimentally by Sinkovits *et al.* [38].

By examining individual chain arrangements, we note that when chains are subjected to large driving amplitudes at relatively high frequencies, the particles oscillate about positions displaced from their static equilibrium configuration.

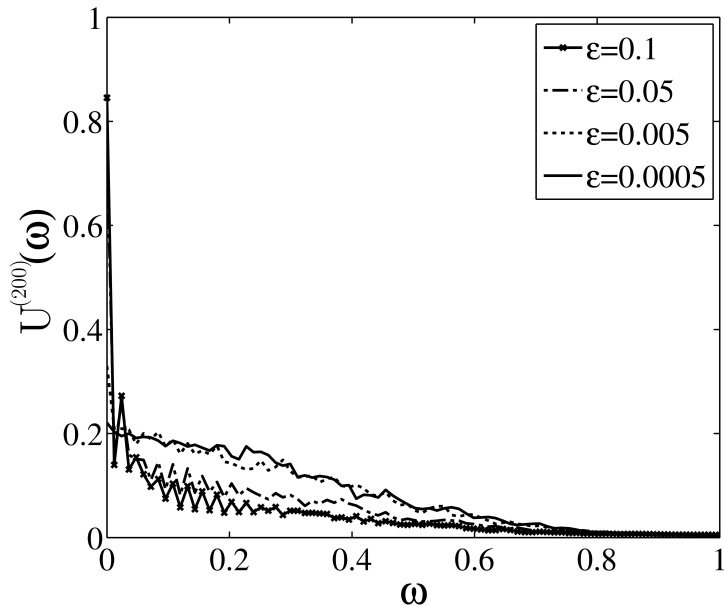


Figure 16: Frequency spectrum at particle $p = 200$ for varied driving amplitude ϵ . Source frequency is $\omega_o = 3.0$ and $\xi = 0.5$.

The input signal induces an additional compression on the chain, displacing all particles from their equilibrium positions (in the positive, “downstream” direction). In the absence of disorder, the particles will then oscillate about the new positions at the driving frequency. Decreasing the frequency of the driver removes this effect and the particles oscillate about their original equilibria.

3.4.2 Removal of contact disorder

In a numerical realization of the monodisperse, mass-disordered setup proposed in Section 2.1.3 we remove the contact disorder in the Hertzian chain by setting all interaction stiffnesses to $\kappa_{ij} = 1$. In Figure 17 we plot the results for the same ensemble of chains with and without contact disorder.

The frequency spectrums of Figures 17a and 17b for $p = 200$ were previously plotted in Figure 13 and inspection of the curves (i) and (ii) reveals no difference due to the removal of contact disorder. Recall that in the linear system, the addition of contact disorder reduced the bandwidth of transmitted frequencies by a small amount.

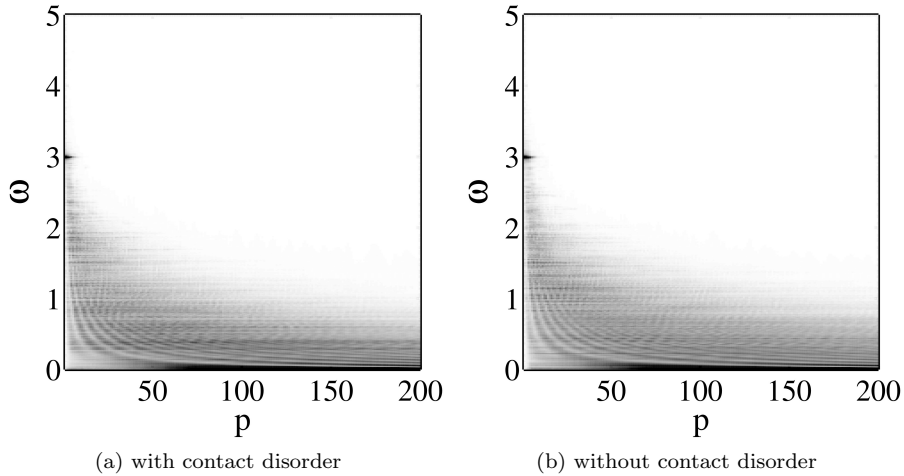


Figure 17: Comparison for contact disorder. $\xi = 0.5$, $\omega_o = 3.0$, and $\epsilon = 0.05$.

4 Conclusions

In this study we examined the frequency transmission properties of driven one-dimensional systems of disordered masses. Beginning from a general power law force-displacement relation, we investigated the behavior of pre-compressed chains where particles interact through linear and nonlinear (Hertzian) contacts. It is shown that disordered chains behave like a low-pass frequency filter, permitting the propagation of low frequency signals while the higher frequency components decay with distance from the source. The rate of decay is studied as a function of the input frequency, disorder magnitude, and the choice of contact model. As more disorder is included in the system we observe that the higher relative frequencies are filtered closer to the source/driver and only low-frequencies propagate in the chain. However, the results also suggest that there exists a threshold disorder after which only small changes in the ensemble-averaged properties are noted. By driving systems at various frequencies we observe that lower-frequency signals are less sensitive to the chain arrangements and the input signal propagates further. In the context of the linear chain, we relate the filtering behavior to the localization of eigenmodes in the presence of disorder.

Comparisons are made for random, linear, contact-ordered chains composed of masses sampled from normal, uniform, and binary distributions. The similarity of the ensemble-averaged results suggest that the moments of the mass distribution are the important parameters for quantifying the disorder and the resulting frequency filtering.

Comparison of the nonlinear and linear systems reveals that both systems filter high frequencies in a similar manner with a decaying envelope of transmitted frequencies. However, the nonlinear chains have frequency spectrums that contain larger relative contributions from the lowest frequency components, indicated by the dramatic difference in the spectrums at locations downstream from the driver. By changing the non-dimensional driving amplitude ϵ we were

able to affect the strength of the nonlinearities present; with a sufficiently small value (corresponding to small driving amplitude and/or large external compression, we recover the linear system behavior.

We examined the effect of isolated mass-disorder and the combination of mass- and contact-disorder in both linear and nonlinear chains. In the linear chain the inclusion of contact disorder was relatively small, leading to a slightly reduced range of transmitted frequencies. Results were qualitatively similar to systems with only mass-disorder. The effect of contact disorder on the Hertzian system is less pronounced; the resulting spectrums do not exhibit noticeable differences.

In comparing the high-frequency filtering properties of the random one-dimensional systems to the three-dimensional packings of Mouraille *et al.* [29] we note the importance of the contact geometry in the resulting behavior. The study performed by Mouraille *et al.* concerned random packings obtained through the introduction of very small perturbations of the particle sizes. Beginning from a perfect crystalline geometry, the variations in particle size created significant disorder effects in the system. The disorder (as quantified here by the distribution of particle masses) was indeed very small ($\xi \approx 0.007$) and our simulations on one-dimensional systems at this disorder reveal no difference from a perfect, monodisperse system. In our consideration of compressed chains, we have avoided geometry induced disorder. However, if the chain were subject to very little pre-compression (approaching Nesterenko's sonic vacuum), the length scale of the particle-size perturbation and the contact overlap length scale would be of the same order and strong nonlinearities could be introduced.

Acknowledgements This research is supported by VICI/NWO-STW.

A Appendix 1: Orthogonality proof

In direct notation, for eigenvalue/eigenvector j the statement of the dimensionless eigenvalue problem is,

$$\mathbf{A}\mathbf{s}_{(j)} = \omega_j^2 \mathbf{s}_{(j)}. \quad (35)$$

With $\mathbf{A} = -\mathbf{M}^{-1}\mathbf{K}$ we have

$$\mathbf{M}^{-1}\mathbf{K}\mathbf{s}_{(j)} = -\omega_j^2 \mathbf{s}_{(j)} \quad (36)$$

or,

$$\mathbf{K}\mathbf{s}_{(j)} = -\omega_j^2 \mathbf{M}\mathbf{s}_{(j)} \quad (37)$$

Similarly for eigenvector k , we have

$$\mathbf{K}\mathbf{s}_{(k)} = -\omega_k^2 \mathbf{M}\mathbf{s}_{(k)} \quad (38)$$

Taking the transpose of (38),

$$\mathbf{s}_{(k)}^T \mathbf{K}^T = -\omega_k^2 \mathbf{s}_{(k)}^T \mathbf{M}^T \quad (39)$$

Since both \mathbf{K} and \mathbf{M} are symmetric drop the transpose and then right multiply by $\mathbf{s}_{(j)}$,

$$\mathbf{s}_{(k)}^T \mathbf{K}\mathbf{s}_{(j)} = -\omega_k^2 \mathbf{s}_{(k)}^T \mathbf{M}\mathbf{s}_{(j)} \quad (40)$$

Similarly, left multiply (37) by $\mathbf{s}_{(k)}^T$

$$\mathbf{s}_{(k)}^T \mathbf{K} \mathbf{s}_{(j)} = -\omega_j^2 \mathbf{s}_{(k)}^T \mathbf{M} \mathbf{s}_{(j)} \quad (41)$$

Subtract (41) from (40),

$$(\omega_j^2 - \omega_k^2) \mathbf{s}_{(k)}^T \mathbf{M} \mathbf{s}_{(j)} = 0 \quad (42)$$

If $\omega_k^2 \neq \omega_j^2$ we are left with the orthogonality statement,

$$\mathbf{s}_{(k)}^T \mathbf{M} \mathbf{s}_{(j)} = 0 \quad (j \neq k) \quad (43)$$

If $j = k$, the quantity $\mathbf{s}_{(j)}^T \mathbf{M} \mathbf{s}_{(j)} = d_{(j)} \neq 0$. Scaling each eigenvector $\mathbf{s}_{(j)}$ by $\sqrt{d_{(j)}}$, we generate an orthonormal set.

B Appendix 2: Hertz contact model

With $\beta = 1/2$ we obtain the Hertz contact model and the interparticle forces are dependent on the size and material properties of the constituent particles in the following way [19]:

$$\tilde{\kappa}_{(i,j)} = \tilde{Y}_{(i,j)} \left[\frac{\tilde{r}_i \tilde{r}_j}{\tilde{r}_i + \tilde{r}_j} \right]^{1/2}, \quad (44)$$

where

$$\tilde{Y}_{(i,j)}^{-1} = \frac{3}{4} \left(\frac{1 - \nu_i^2}{\tilde{E}_i} + \frac{1 - \nu_j^2}{\tilde{E}_j} \right). \quad (45)$$

\tilde{E}_i and ν_i are the elastic modulus and Poisson's ratio, respectively, of the material composing particle i . The formulation was presented for spheres but is noted to be appropriate for non-spheres as well [19]. In what follows we choose the same material for all particles and $\tilde{Y}_{(i,j)} = \tilde{Y}$ is independent of the contact in consideration,

$$\tilde{Y}^{-1} = \frac{3}{2} \left(\frac{1 - \nu^2}{\tilde{E}} \right). \quad (46)$$

We have previously defined the characteristic length $\tilde{\ell} = \tilde{\Delta}_o$ to be the equilibrium contact overlap of two particles of the mean mass \tilde{m}_o . We first find the characteristic stiffness of this contact,

$$\tilde{\kappa}_o = \frac{\tilde{E}}{1 - \nu^2} \left[\frac{2\tilde{m}_o}{243\pi\tilde{\rho}} \right]^{1/6}. \quad (47)$$

With the initial overlaps defined by (3), we have,

$$\tilde{\Delta}_o = \left(\frac{\tilde{P}}{\tilde{\kappa}_o} \right)^{2/3} \quad (48)$$

The characteristic time is,

$$\tilde{t}_c = \frac{1}{\tilde{\Delta}_o^{1/4}} \sqrt{\frac{1 - \nu^2}{\tilde{E}}} \left[\frac{243\pi\tilde{\rho}\tilde{m}_o^5}{2} \right]^{1/12}. \quad (49)$$

The scaled stiffness ratio at contact (i, j) simplifies to,

$$\kappa_{(i,j)} = \frac{\tilde{\kappa}_{(i,j)}}{\tilde{\kappa}_o} = \sqrt{\frac{2}{b^{(i)1/3} + b^{(j)1/3}} \left(b^{(i)}b^{(j)}\right)^{1/6}}. \quad (50)$$

For a general contact, the equilibrium overlap given by (3) is,

$$\tilde{\Delta}_{(i,j)} = \left(\frac{\tilde{P}}{\tilde{\kappa}_{(i,j)}}\right)^{2/3}. \quad (51)$$

Dividing by our length scale $\tilde{\Delta}_o$, the characteristic contact overlap in equilibrium,

$$\Delta_{(i,j)} = \kappa_{(i,j)}^{-2/3}. \quad (52)$$

References

- [1] J.D. Anderson. *Principles of the Theory of Solids*. Cambridge University Press, 2nd edition, 1972.
- [2] P.W. Anderson. Absence of diffusion in certain random lattices. *Phys. Rev.*, 109(5):1492–1505, 1958.
- [3] C. Coste and B. Gilles. On the validity of hertz contact law for granular material acoustics. *Eur. Phys. J. B*, 7:155–168, 1999.
- [4] C. Daraio, V.F. Nesterenko, E.B. Herbold, and S. Jin. Energy trapping and shock disintegration in a composite granular medium. *Phys. Rev. Lett.*, 96:058002, 2006.
- [5] P. Dean. On disordered one-dimensional crystals. *Proc. Phys. Soc.*, 73:413–421, 1959.
- [6] R.L. Doney and S. Sen. Impulse absorption by tapered horizontal alignments of elastic spheres. *Phys. Rev. E*, 72:041304, 2005.
- [7] Robert Doney and Surajit Sen. Decorated, Tapered, and Highly Nonlinear Granular Chain. *Physical Review Letters*, 97(15):APS–4.
- [8] F.J. Dyson. The dynamics of a disordered linear chain. *Phys. Rev.*, 92(6):1331–1338, 1953.
- [9] F. Fraternali, M.A. Porter, and C. Daraio. Optimal design of composite granular protectors. *Mech. Adv. Mater. Struct.*, 17:1–19, 2010.
- [10] M. Gharib, A. Celik, and Y. Hurmuzlu. Shock absorption using linear particle chains with multiple impacts. *J. Appl. Mech.*, 78(3):031005, 2011.
- [11] H.E. Hall. *Solid State Physics*. John Wiley & Sons Ltd., London, 1974.
- [12] U. Harbola, A. Rosas, A.H. Romero, M. Esposito, and K. Lindenberg. Pulse propagation in decorated granular chains: an analytical approach. *Phys. Rev. E*, 80:051302, 2009.

- [13] U. Harbola, A. Rosas, A.H. Romero, and K. Lindenberg. Pulse propagation in randomly decorated chains. *Phys. Rev. E*, 82:011306, 2010.
- [14] E.B. Herbold, J. Kim, V.F. Nesterenko, S.Y. Wang, and C. Daraio. Pulse propagation in a linear and nonlinear diatomic periodic chain: effects of acoustic frequency band-gap. *Acta Mech.*, 205:85–103, 2009.
- [15] X. Jia, C. Caroli, and B. Velicky. Ultrasound propagation in externally stressed granular media. *Physical Review Letters*, 82(9):1863–1866, 1999.
- [16] S. Job, F. Melo, A. Sokolow, and S. Sen. Solitary wave trains in granular chains: experiments, theory, and simulations. *Gran. Matt.*, 10:13–20, 2007.
- [17] J.A. Judge, B.H. Houston, D.M. Photiadis, and P.C. Herdic. Effects of disorder in one- and two-dimensional micromechanical resonator arrays for filtering. *Journal of Sound and Vibration*, 290:1119–1140, 2006.
- [18] E. Kreyszig. *Advanced Engineering Mathematics*. John Wiley & Sons Inc., New York, 1999.
- [19] L. Landau and E. Lifschitz. *Theory of elasticity*. MIR, Moscow, 1967.
- [20] M. Leibig. Model for the propagation of sound in granular materials. *Phys. Rev. E*, 49(2):1647–1656, 1994.
- [21] E.H. Lieb and D.C. Mattis. *Mathematical Physics in One Dimension. Exactly soluble models of interacting particles*. Academic Press, New York, 1966.
- [22] S. Luding, E. Clément, A. Blumen, J. Rajchenbach, and J. Duran. Studies of columns of beads under external vibrations. *Phys. Rev. E*, 49(2):1634, 1994.
- [23] M. Manciu, S. Sen, and A. J. Hurd. The propagation and backscattering of soliton-like pulses in a chain of quartz beads and related problems. (i). Propagation. *Physica A*, 274:588–606, 1999.
- [24] M. Manciu, S. Sen, and A. J. Hurd. The propagation and backscattering of soliton-like pulses in a chain of quartz beads and related problems. (ii). Backscattering. *Physica A*, 274:607–618, 1999.
- [25] M. Manciu, S. Sen, and A.J. Hurd. Impulse propagation in dissipative and disordered chains with power-law repulsive potentials. *Physica D*, 157:226–240, 2001.
- [26] F. Melo, S. Job, F. Santibanez, and F. Tapia. Experimental evidence of shock mitigation in a hertzian tapered chain. *Phys. Rev. E*, 73:041305, 2006.
- [27] E.W. Montroll and R.B. Potts. Effect of defects on lattice vibrations. *Phys. Rev.*, 100(2):525–543, 1955.
- [28] O. Mouraille. *Sound propagation in dry granular materials: discrete element simulations, theory, and experiments*. PhD thesis, Universiteit Twente, 2009.

- [29] O. Mouraille and S. Luding. Sound wave propagation in weakly disperse polydisperse granular materials. *Ultrasonics*, 48(6–7):498–505, 2008.
- [30] V. F. Nesterenko. Propagation of nonlinear compression pulses in granular media. *J. Appl. Mech. Tech. Phys.*, 24(5):733–743, 1983.
- [31] L. Ponsou, N. Boechler, Y.M. Lai, M.A. Porter, P.G. Kevrekidis, and C. Daraio. Nonlinear waves in disordered diatomic granular chains. *Physical Review E*, 82:021301, 2010.
- [32] T. Pöschel and N. V. Brilliantov. Extremal collision sequences of particles on a line: optimal transmission of kinetic energy. 2000.
- [33] H.B. Rosenstock and R.E. McGill. Vibrational modes of disordered linear chains. *J. Math. Phys.*, 3(1):200–202, 1962.
- [34] H. Schmidt. Disordered one-dimensional crystals. *Phys. Rev.*, 105(2):425–441, 1957.
- [35] S. Sen, J. Hong, J Bang, E. Avalos, and R. Doney. Solitary waves in the granular chain. *Physics Reports*, 462:21–66, 2008.
- [36] S. Sen, M. Manciu, and J.D. Wright. Solitonlike pulses in perturbed and driven hertzian chains and their possible applications in detecting buried impurities. *Physical Review E*, 57(2):2386–2397, 1998.
- [37] P. Sheng. *Introduction to Wave Scattering, Localization and Mesoscopic Phenomena*. Springer Verlag, Berlin, 2006.
- [38] R. S. Sinkovits and S. Sen. Nonlinear Dynamics in Granular Columns. *Phys. Rev. Lett.*, 74(14):2686, 1995.
- [39] A. Sokolow, J.M. Pfannes, R.L. Doney, M. Nakagawa, J.H. Agui, and S. Sen. Absorption of short duration pulses by small, scalable, tapered granular chains. *Appl. Phys. Lett.*, 87:254104, 2005.
- [40] V. Tournat, V.E. Gusev, and B. Castagnède. Self-demodulation of elastic waves in a one-dimensional granular chain. *Physical Review E*, 70(2):056603, 2004.
- [41] D.T. Wu. Conservation principles in solitary impulse propagation through granular chains. *Physica A*, 315:194–202, 2002.